Preprints (www.preprints.org) | NOT PEER-REVIEWED | Posted: 22 May 2023 doi:10.20944/preprints202305.1502.v1

Disclaimer/Publisher's Note: The statements, opinions, and data contained in all publications are solely those of the individual author(s) and contributor(s) and not of MDPI and/or the editor(s). MDPI and/or the editor(s) disclaim responsibility for any injury to people or property resulting from any ideas, methods, instructions, or products referred to in the content.

Article

Hydrothermally synthesized ZnMgAl-layered double hydroxide and rice husk biochar composites for Cu(II) and Pb(II) ions removal from synthetic wastewater

M. Shafiq [1,*], A.A. Alazba [1,2] and M.T. Amin [1,3,*]

[1] Alamoudi Water Research Chair, King Saud University, P. O. Box 2460, Riyadh 11451, Kingdom of Saudi Arabia.
[2] Agricultural Engineering Department, King Saud University, P. O. Box 2460, Riyadh 11451, Kingdom of Saudi Arabia.
[3] Department of Environmental Sciences, COMSATS University Islamabad, Abbottabad Campus, Abbottabad 22060, Pakistan.
* Correspondence: msrana@ksu.edu.sa (M.S.); mtamin@ksu.edu.sa (M.T.A.)

Abstract: The efficiency of a new composite material of the layered double hydroxide (LDH) of ZnMgAl and rice husk biochar (RHB) for the removal of Cu(II) and Pb(II) ions from synthetic wastewater was investigated in this study. The images of scanning electron microscope showed extremely fine crystalline LDH particles decorated on the rough surface of the RHB while the succesful formation of the composite adsorbent (LDH/RHB) was confirmed by the corresponding energy dispersive X-ray and the Fourier-transform infrared spectroscopy. An equilibrium contact time of 30 and 15 min for Cu^{2+} and Pb^{2+}, respectively, was proposed for the optimum performance of the batch adsorption process. The dose of the LDH/RHB adsorbent was optimized at 0.4 g yielding maximum adsorption capacities of 117 and 124 mg g^{-1} for Cu^{2+} and Pb^{2+}, respectively, with corresponding maximum removal efficiencies of nearly 94% and 99%. The initial meta concentrations was optimized at 50 or 60 mg L^{-1} corresponding to maximum removal efficiencies or adsorption capacities. For the changing initial metal's concentration, the removal efficiencies remained unchanged for up to 50 mg L^{-1} and decreased by about 50% by increasing the initial concentrations from 50 to 100 mg L^{-1}. The adsorption capacities observed a linear increasing trend by increasing the initial concentrations from 5 to 60 mg L^{-1} and remained unchanged afterward up to 100 mg L^{-1}. A solution pH of 6.0 yielded optimum results with an increasing trend in adsorption capacities and percentage removal by changing the solution pH from 2.0 to 7.0. Based on the best-fit of the pseudo second-order kinetic model to the experimental data, the chemisorption was suggested to be the controlling mechanism of adsorption. The fitting of the Langmuir model suggested a monolayer sorption of Cu^{2+} and Pb^{2+} in addition to a heterogeneous adsorption as supported by the fitting of the Temkin isotherm. The application of the Dubinin–Radushkevich isotherm proposed a physical adsorption (mean free energy of adsorption less than 8 kJ mol^{-1}) of both heavy metal ions on the surface of the LDH/RHB adsorbent.

Keywords: Batch adsorption; Langmuir isotherm; LDH/RHB; pseudo second-order

Introduction

Rising concentrations of toxic pollutants and chemicals in surface and other available fresh water reservoirs have become a major concern worldwide, simply because of the expansion of industrial and anthropogenic activities [1]. Heavy metals with higher concentrations, such as copper (Cu) and lead (Pb), are of particular concern because these are predominantly used in industry and are extremely detrimental to human health and also for aquatic creatures [2]. In humans, acute Pb poisoning has devastating effects on the kidneys, brain, liver and central nervous system. Copper is undoubtedly a vital trace element for all living things, but its presence in large amounts could be

© 2023 by the author(s). Distributed under a Creative Commons CC BY license.

Preprints (www.preprints.org) | NOT PEER-REVIEWED | Posted: 22 May 2023 doi:10.20944/preprints202305.1502.v1

harmful to humans and may result in nausea, vomiting, and abdominal discomfort [3,4]. Thus, it is imperative that efficient methods and legislations must be developed to regulate the untreated discharge of industrial wastewater into fresh water reservoirs, in order to safeguard humanity from these possible harmful impacts.

Development of innovative technologies to purify industrial effluent before it is released into waterways are need of the time. Microbial (microalgae) fuel cell technology, membrane technology and solar irradiation are some of the new wastewater treatment technologies that have yet to mature [5–7]. Reverse osmosis, chemical precipitation, ion exchange, and adsorption are just a few well-known technologies that have been frequently used in order to eradicate heavy metals from industrial wastewater [8,9]. So far, adsorption is the best and most practical technology to treat industrial wastewater. In adsorption process, the selection of adsorbent plays an important role in achieving maximum efficiency [10]. In recent years, biochar (BC), activated carbon, clay composites, nanomaterials and layered double hydroxides (LDHs) have provided the best results for Cu(II) and Pb(II) ions remediation in wastewater [11–19].

The term "biochar" refers to a carbon-rich porous solid material made from biomass waste through pyrolysis in a reactor at moderate temperature (e.g., 400-700°C) in the absence or presence of minimal oxygen [20]. The yield and quality of BC depends on the type of feedstock used for pyrolysis conditions due to the catalytic effects during pyrolysis. Agricultural waste biomass is one of the most valuable and renewable sources for BC production. This is because agricultural waste biomass has a higher lignin-to-cellulose ratio, which results in a high carbon byproduct [21]. For instance, rice husk is a frequently available byproduct of the rice milling business, accounting for around 20% of the whole mass of rice products [22,23]. As there is currently no appropriate use for this waste, it could be a good raw material for BC production. Sanka et al. [24] prepared BC from rice husk and claimed 90% removal of Pb(II) and other heavy metals. However, the adsorption performance of BC is still limited because of the low specific surface area and porosity [25]. Consequently, modifying and functionalizing pristine BC into superior composite materials with unique structures and surface characteristics is, thus, a key approach to diversifying its uses [26]. In the process of pursuing this goal, BC is currently being used as a substrate in composites with other superior adsorbents such as carbon nanotube, graphene, metal organic framework and layered double hydroxide (LDH), substantially tripling the adsorption capacity that was previously accessible individually [27,28].

The LDHs are a class of materials that are similar to hydrotalcite, an anionic clay with a positively charged host layer, and the counter anion located in the interlayer region, with the general formula $[M^{2+}_{1-x}M^{3+}_{x}\ (OH^{-})_2]^{x+}\ (A^{n-})_{x/n}.\ mH_2O$, where M^{2+} and M^{3+} represent divalent and trivalent cations, respectively, A^{n-} denotes a guest interlayer charge balancing anion, and x symbolizes the proportion of trivalent metal ions, which might vary depending on the type of application [3]. LDHs are highly porous, and possess unique super molecule structure, large specific surface area, withstand high temperatures, controllable element composition, and are efficient ion exchanger [29]. Moreover, LDH-based catalysts have widely been used in the fields of environmental remediation because of their advantageous properties, such as low cost, long-lasting stability, high catalytic performance, and distinctive structural characteristics (such as intercalation, and the ability to be coupled with other useful materials) [30]. There are many synthesis methods for LDHs production, each of which can modify the properties of the final product to make it more or less suitable for specific applications [31]. The most common technique is the coprecipitation method. However, poor porosity development and high leaching rate in the reaction process have limited the production of LDHs and it is utilized as a contaminants removal adsorbent [32]. Consequently, it is essential to discover methods of treating LDHs deficiency in order to advance the development and increase their applications. Therefore, to fill this gap, porous BC is an ideal carrier matrix for the appropriate coating of LDHs, providing a large reactive surface area and preventing their aggregation [33]. As a result, combining LDHs with BC is a win-win approach for both LDHs and BC in terms of property enhancement [26].

Preprints (www.preprints.org) | NOT PEER-REVIEWED | Posted: 22 May 2023 doi:10.20944/preprints202305.1502.v1

In recent years, composite materials based on BC and LDHs have opened up new areas of investigation into optimizing and accelerating the removal of pollutants. Several studies have been conducted on the mechanism of heavy metal adsorption by BC-supported LDHs composites. For example, *Tan et al.* [34] prepared a composite of Zn-Fe-LDH and kiwi branch BC (KB/Zn-Fe) for the mitigation of Pb(II) ions from aqueous solution and claimed an adsorption capacity of 161.29 mg g^{-1}, compared to 36.76 mg g^{-1} for the original BC. *Jia et.al* [35] synthesized a MgFe-LDH and magnetic BC for the removal of Pb(II) from aqueous solution and they observed maximum adsorption capacity of 476.25 mg g^{-1}. *Wang et al*. [4] produced MnAl-LDH and BC composite for the attenuation of Cu(II) ions and they observed adsorption capacity of 74.04 mg g^{-1}. *Khandaker et.al* [36] prepared a composite of MgFe-LDH and bamboo waste charcoal for the remediation of Cu(II) ions from wastewater and found an adsorption capacity of 85.47 mg g^{-1}. However, there is a limited number of studies exploring the remediation mechanism of BC supported LDHs composites for heavy metals removal from wastewater.

Thus, the specific goal of this study was to develop a new composite material of ZnMgAl(LDH) and rice husk BC (RHB) using the co-precipitation and hydrothermal technique and to investigate the removal mechanisms of Cu(II) and Pb(II) ions from synthetic wastewater. A number of batch experiments were performed to probe the effectiveness of the newly created composite material in removing the targeted heavy metals. Moreover, the kinetics and isothermal models were deployed to understand the removal mechanisms and to calculate the adsorption capacity of the composite material. The scanning electron microscopy (SEM), energy dispersive X-ray (EDX) spectroscopy, and Fourier-transform infrared spectroscopy (FTIR) techniques were employed to analyze the morphology and the presence of various functional groups on the surface of composite material.

2. Materials and procedures

2.1. chemicals and batch testing

Copper nitrate trihydrate ($Pb(NO_3)_2.3H_2O$) and lead nitrate ($Pb(NO_3)_2$, as purchased from Tianjin Benchmark, China were used respectively to prepare the stock solutions of Cu^{2+} and Pb^{2+}). The required amount of both salts was added in deionized water for this purpose which was used further to prepared the dilutions, as required in different batch tests, in obtaining the intended initial concentration of each metal ion. 0.1M of analytical grade HCl and NaOH were used to set and maintain the required pH of the solution.

Two different volumes of sample solutions (50 or 100 mL) containing the required initial concentrations of Cu^{2+} or Pb^{2+} were used for the batch tests and the desired amount of the adsorbents was added accordingly. The conical flasks containing the tested dilutions were placed inside a temperature-controlled shaker (Wise Cube orbital, Wisd. ThermoStable IS-20, Daihan Scientific Co. Ltd., South Korea) operating at 30 °C and 220 rpm. After agitating for a selected contact time, the diluted solution was withdrawn from the shaker and filtered through a 0.45 µm Whatman™ filter. A flame atomic absorption was employed for measuring the residual concentration of each metal after a 5 mL of the filtered sample was inserted inside FAAS. The percentage removal and the adsorption capacity (q_t, mg g^{-1}) of either of the Cu^{2+} or Pb^{2+} is measured as follows;

$$Percentage\ removal\ (\%) = \left(\frac{C_0 - C_t}{C_0}\right) \times 100 \quad (1)$$

$$Adsorption\ capacity = \left(\frac{C_0 - C_t}{m}\right) V \quad (2)$$

where C_0 and C_t (both measured in mg L^{-1}) is the selected initial metal concentration and the residual metal concentration, as measured using FAAS, respectively. The quantity of the adsorbent material (g) and the volume of the tested dilutions (L) is presented by measured in m and V and in Eq. 2, respectively.

Preprints (www.preprints.org) | NOT PEER-REVIEWED | Posted: 22 May 2023 doi:10.20944/preprints202305.1502.v1

2.2. Preparation of the rice husk biochar and the composite adsorbent

The waste of rice husk was collected locally to make the rice husk biochar (RHB) to be used in preparing the composite adsorbent. Prior to a three-day drying in open (under sunlight), impurities (dust particles etc.) were removed from the collected mass by washing multiple times with clean water. The dried mass was crushed in small pieces with an average particle size in the range 2 – 3 cm which were inserted in a muffle furnace (operating at 500℃ at a ramp rate of 5℃/ min^{-1}) in the absence of oxygen for pyrolysis for nearly five hours. The pyrolyzed product was washed with pure water to remove the ash, dried in an oven for about a day at 100℃, and subsequently crushed in a ball mill to get nano scale particles of RHB.

Co-precipitation method and hydrothermal technique was used to prepare the composite adsorbent of ZnMgAl(LDH) and RHB. To prepare the LDH of ZnMgAl, 1.071 g (0.06 mol) of zinc nitrate hexahydrate ($Fe(NO_3)_3.6H_2O$), 1.846 g (0.12 mol) of magnesium nitrate hexahydrate ($Mg(NO_3)_2.6H_2O$), and 0.675 g (0.03 mol) of aluminum nitrate nonahydrate ($Al(NO_3)_3.9H_2O$) were added in 60 mL of deionized water inside a beaker. The mixture was constantly stirred for about an hour to ensure that all of the salts were completely dissolved. After complete dissolution, this solution was shifted to another beaker which contains 0.6 g of nano-sized RHB under constant stirring. Afterwards, a solution of NaOH (0.5 M) and Na_2CO_3 (0.125 M) was dripped through burette till the solution pH reached around 10. The resulting slurry was then stirred for another two hours before transferring to hydrothermal reactor and kept in an oven for almost 24 hours at 180℃. After cool down, the slurry solution was transferred to centrifuge tube operating at 5000 rpm to separate the particles. This procedure was repeated five times to wash the resulting material with deionized water. After washing, the composite material was kept in an oven for 24 hours at 75℃ for drying purpose.

The characterization of the RHB, ZnMgAl(LDH) and the composite adsorbent (LDH/RHB) before adsorption and that of the composite adsorbent after adsorption of both heavy metal ions is performed using the SEM, EDX, and the FTIR techniques.

3. Results and discussions

3.1. Adsorbents' properties and the mechanism of adsorption

3.1.1. Surface morphology and elemental composition analysis

Fig. 1 shows the findings of SEM and EDX analysis performed on samples of RHB, ZnMgAl(LDH), and LDH/RHB composites. The SEM micrographs of RHB revealed agglomerated mass, angular, dense, and flake sharply-edged particles of the parent biochar, whereas EDX revealed the evidence of carbon (51.17%), oxygen (35.36%), and other minerals on BC surface [37]. Similar to this, SEM micrographs of ZnMgAl(LDH) exhibited very prominent hexagonal platelet structures as well as some nanorods-like structures [3,38]. In addition, the distribution of metal elements such as carbon, oxygen, magnesium, zinc, and aluminum were precisely displayed in the EDX spectrums, indicating that the synthesized LDHs had excellent purity [39]. Similarly, highly magnified SEM micrographs of the LDH/RHB composite showed extremely fine crystalline LDH particles decorated on the rough surface of the RHB. To prove that the composite was successfully formed, the corresponding EDX spectrum of the composite displays all bonding elements that were present separately in the RHB and ZnMgAl(LDH) spectra. Therefore, the characterizations indicated that ZnMgAl(LDH) was effectively incorporated into the surface of RHB.

Preprints (www.preprints.org) | NOT PEER-REVIEWED | Posted: 22 May 2023 doi:10.20944/preprints202305.1502.v1

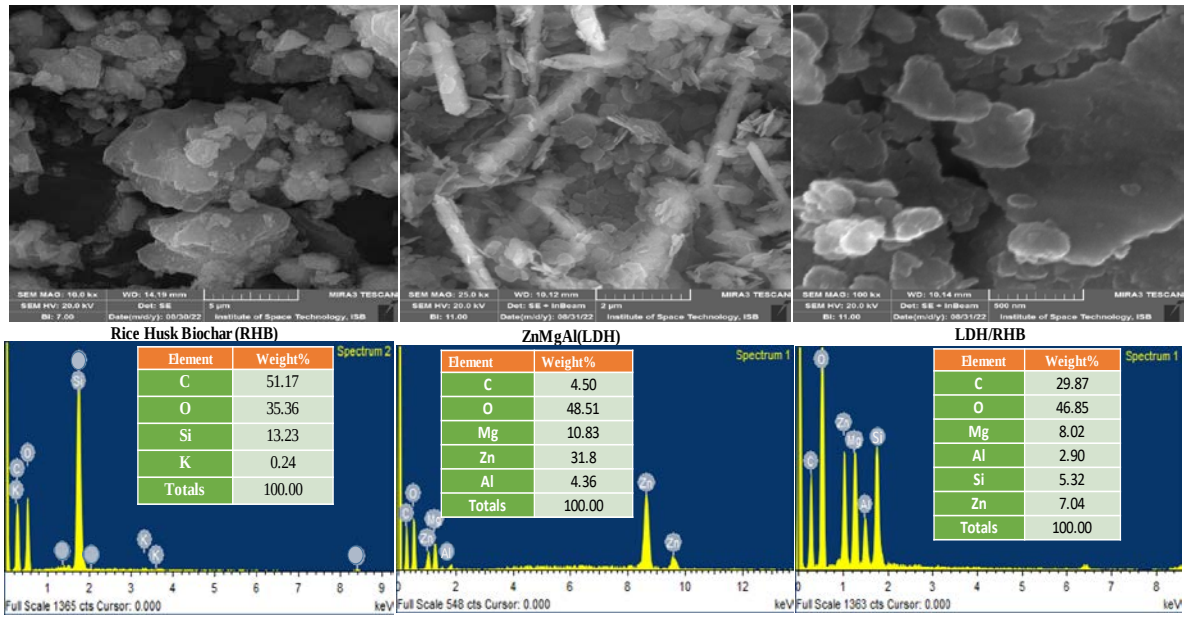

Figure 1. SEM and EDX micrographs of Rice Husk Biochar (RHB), ZnMgAl(LDH) and the composite compound (LDH/RHB).

SEM-EDX analysis of the LDH/RHB composite after Cu^{2+} and Pb^{2+} absorption (Fig. 2) showed that the composite surface becomes brighter and very small precipitates appeared on the surface, which could be due to the formation of Pb- and Cu-hydroxides and other metal compounds [40]. This statement was confirmed by the EDX spectra of LDH/RHB–Cu^{2+} and LDH/RHB–Pb^{2+}, which showed many variations in elemental composition and the presence of Cu (3.41%) and Pb (47.63%), which may indicate successful absorption of the target metals into the LDH/RHB composite [41,42].

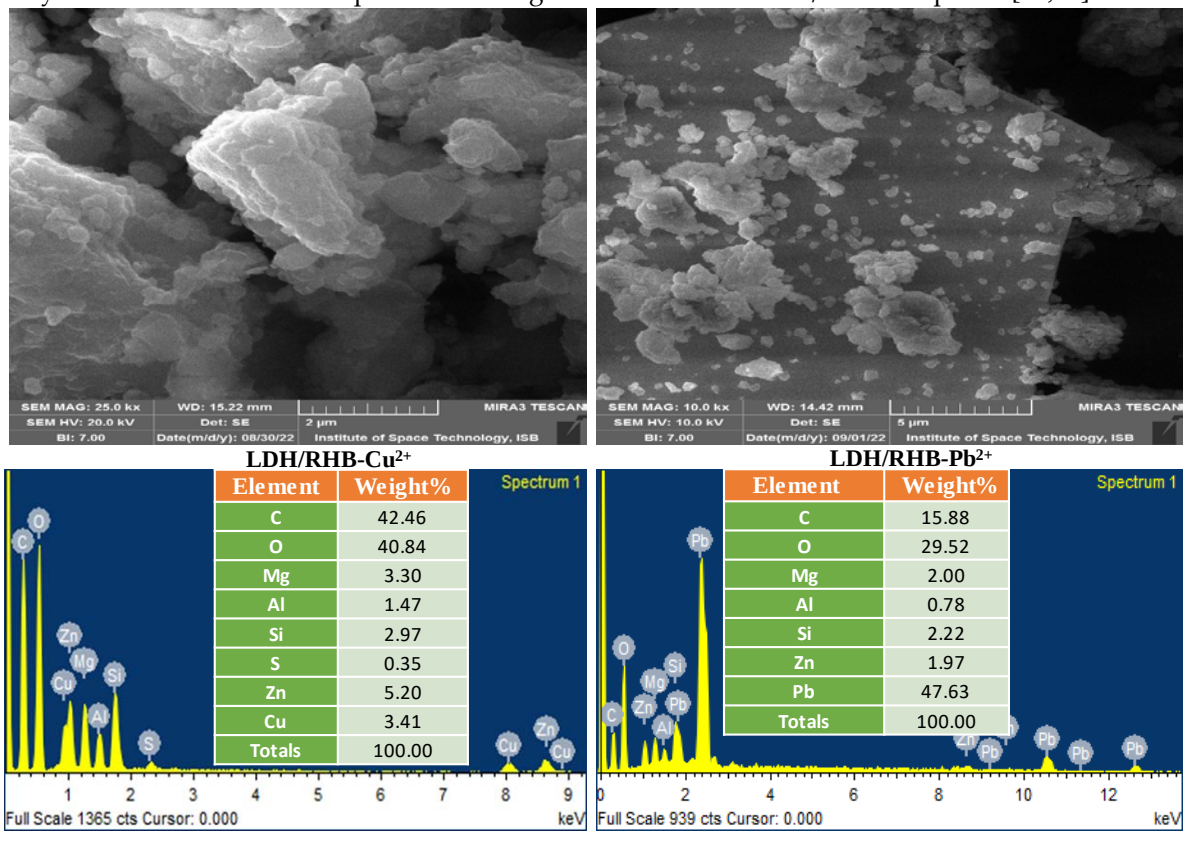

Figure 2. SEM and EDX images of Rice Husks Biochar (RHB) and ZnMgAl(LDH) composites (LDH/RHB) after Cu^{2+} and Pb^{2+} adsorption.

Preprints (www.preprints.org) | NOT PEER-REVIEWED | Posted: 22 May 2023 doi:10.20944/preprints202305.1502.v1

3.1.2. Fourier transform infrared analysis

The presence and changes in functional groups on the surface of RHB, ZnMgAl(LDH) and LDH/RHB composites were investigated using FTIR spectra before and after adsorption of Cu^{2+} and Pb^{2+}, as shown in Fig. 3. The wavenumber range of 4000 to 400 cm^{-1}, where most of the changes in the FTIR spectra between analyzed samples were observed. The spectrum of RHB in Fig. 3d showed a broad absorption band around 3300-3650 cm^{-1} and the distinctive peak at 1602 cm^{-1}, which is associated with the bending and stretching vibration of O-H groups and interlayer water molecules in the tested material structure [38,43]. In addition, the RHB spectrum's most obvious point is at 1070 and 799 cm^{-1}, which corresponds to Si-O-Si or Si-O, demonstrating the high Si content of RHB [44].

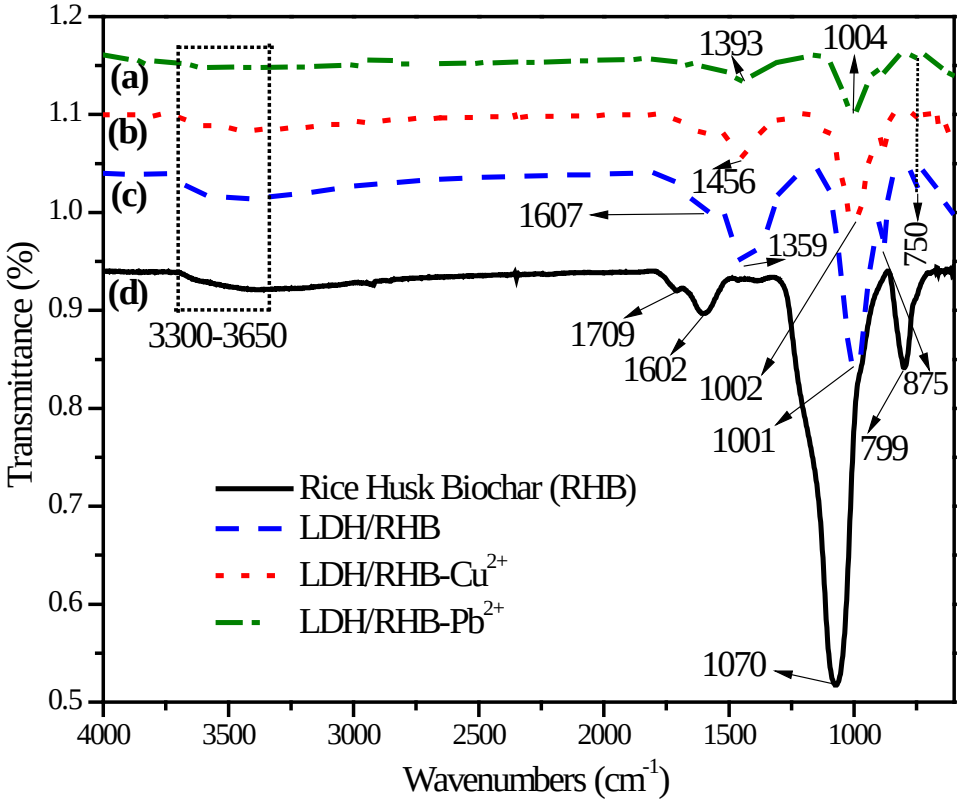

Figure 3. FT-IR spectra of Rice Husk Biochar (RHB), ZnMgAl(LDH) and their composite (LDH/RHB) before and after adsorption of copper (LDH/RHB-Cu^{2+}) and lead (LDH/RHB-Pb^{2+}).

Fig. 3c showed the spectra of the LDH/RHB composite, revealing that the distinctive band at about 1359 cm^{-1} is linked to the stretching vibration mode of NO^{-3} [45,46]. Another, prominent set of band shift was noticed from 1070 to 1001 cm^{-1} and 799 to 750 cm^{-1} in the spectra of LDH/RHB composite, which symbolizes the stretching vibration of Si-O-Si or Si-O, but their intensity was significantly reduced compared to that obtained in Fig. 3c. A new weak band was appeared at 875 cm^{-1} in the spectra of LDH/RHB composite, which could correspond to metal-oxygen (M-O or M-O-M) vibrations [47,48]. Hence, the effective synthesis of the LDH/RHB composites is evidenced in these analyses. Furthermore, the FTIR spectrum after adsorption of Cu^{2+} (Fig. 3b) and Pb^{2+} (Fig. 3a) onto the LDH/RHB composite, indicated a band shift from 1001 to 1002 and 1004 cm^{-1}, respectively. More importantly, nitrate and hydroxyl representing bands may change (low intensity) or vanished, suggesting that these groups were replaced by $Cu^{2+}$and Pb^{2+}, as illustrated in Figs. 3b 3a, respectively.

3.2. Estimation of the equilibrium contact time and optimization of the parameters of batch adsorption

The equilibrium contact time was determined by monitoring variations in adsorption capacity and removal efficiencies in order to maximize the performance of the examined adsorption system and for effective adsorbent consumption. Fig. 4 shows these changes within a suitable time range (0

Preprints (www.preprints.org) | NOT PEER-REVIEWED | Posted: 22 May 2023 doi:10.20944/preprints202305.1502.v1

– 300 min) for 50 and 80 mg L^{-1} of both heavy metal ions using 0.4 g of the composite adsorbent (LDH/RHB) by maintainign the solution pH at 6.0±0.3. A similar trend of rapid uptake of each heavy metal ion upon immediate contact with the adsorbent having abundant free active sites, was observed irrespective of the initial concentration (50 or 80 mg L^{-1}, as shown in Fig. 4a and 4b, respectively). For Cu^{2+}, steady increase in the adsorption capacity continued until 30 min while the same was seen for Pb^{2+} until 15 min of the contact time. A different equilibrium contact time, thus, was proposed for Cu^{2+} and Pb^{2+} for the optimal performance of the adsorption system. Due to the unavailability or saturation of the free active sites at the surface of the LDH/RHB adsorbent, no changes in the adsorption capacity or removal efficiency were seen for Pb^{2+} after 15 min while for 50 mg L^{-1} of Cu^{2+}, both parameters increased slightly upto 60 minutes of contact time (Fig. 4a). The studied adsorbent exhibited slightly higher adsorption capacity and removal efficiency for Pb^{2+} in comparison to Cu^{2+} in addition to the half retention time for an optimal performance. For 50 mg L^{-1} of both heavy metal ions, the optimal values for the adsorption capacity and removal efficiency were 117 mg g^{-1} and 94%, respectively, for Cu^{2+} at 30 min whereas for Pb^{2+}, these values were recorded as 124 mg g^{-1} and 99%, respectively at 15 min.

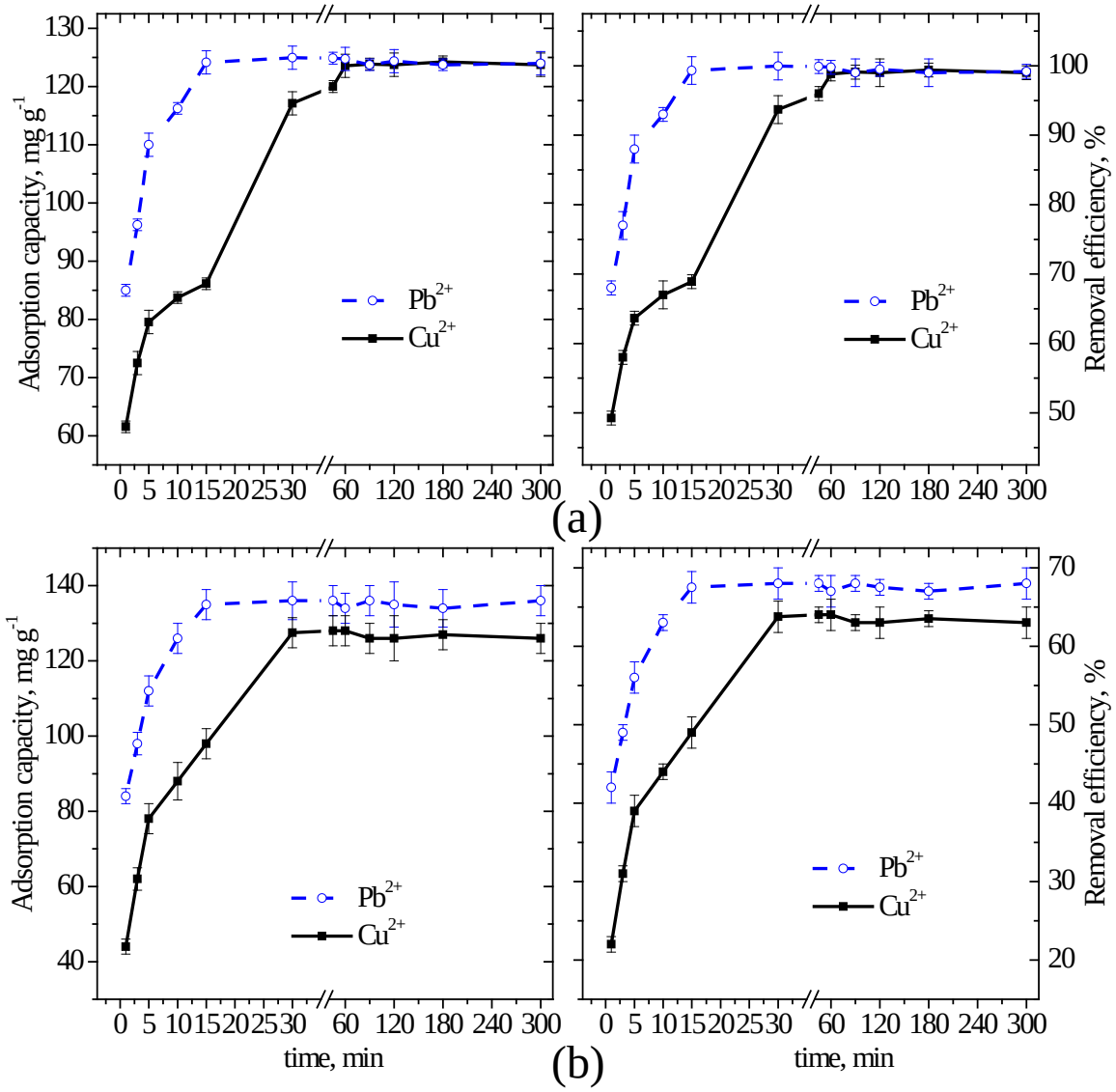

Figure 4. Variations with time in the uptake capacity and percentage removal at 50 (a) and 80 mg L^{-1} (b)of both heavy metal ions using the composite compound

Among the several parameters influencing the effectiveness of batch adsorption process, the amount of the LDH/RHB adsorbent was customised by identifying the variations in the adsorption

Preprints (www.preprints.org) | NOT PEER-REVIEWED | Posted: 22 May 2023 doi:10.20944/preprints202305.1502.v1

capacities and removal efficiencies of both heavy metal ions at various initial doses of the adsorbent (0.05 – 0.7 g), as shown in Fig. 5. Batch tests were performed at already determined equilibrium contact time of 30 and 15 min for Cu^{2+} and Pb^{2+}, respectively, under a maintained solution pH of 6.0±0.3 and 50 mg L^{-1} as a constant initial concentration for each heavy metal ion. For either heavy metal ion, a steady increase in the adsorption capacity can be seen reaching to maximum values of 117 and 124 mg g^{-1} for Cu^{2+} and Pb^{2+}, respectively, at 0.4 g of the tested dose of the LDH/RHB adsorbent. The removal efficiency was also maximum (more than 99%) for Pb^{2+} at 0.4 g of the LDH/RHB adsorbent while 94% of removal efficiency was recorded for Cu^{2+} at this value which further increased to about 99.9% at maximum tested dose (0.8 g) of the LDH/RHB adsorbent. Increase in the adsorption capacity was probably due to the availability of more active sites with increasing amount of the adsorbent to absorb a fixed concentration of the absorbent (50 mg L^{-1} of each metal ion). After attaining the maximum removal efficiency (about 99%) at 0.4 g of the LDH/RHB adsorbent as a result of more exchangeable adsorption sites with increasing amount of the adsorbent, the uptake capacity started decreasing due to unused adsorbent beyond 0.4 g and hence, rendered it to be the optimum LDH/RHB adsorbent value for optimal performance of the investigated adsorption process.

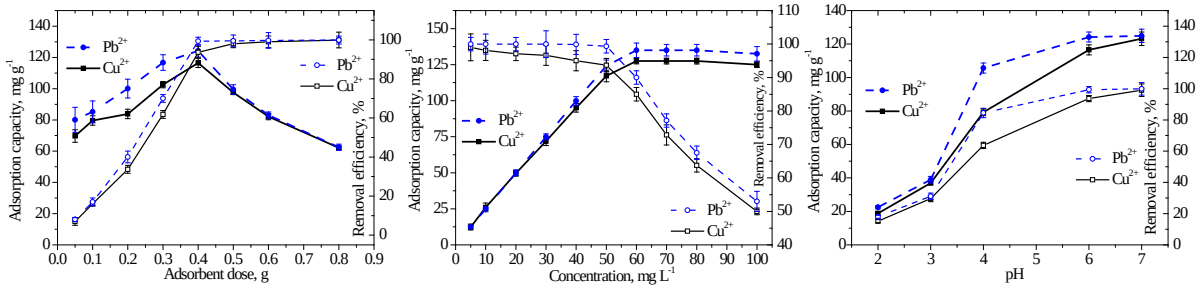

Figure 5. Variations in the uptake capacity and the percentage removal of both heavy metal ions by changing the dose of the adsorbent, initial concentrations of each metal and the solution pH.

Variations in the adsorption capacities and the removal efficiencies by varying the initial concentrations of both heavy metal ions in the range 5 – 100 mg L^{-1} are shown in Fig. 5. Batch process was optimized in this regard by using 0.4 g of the LDH/RHB adsorbent under a maintained solution pH of 6.0±0.3 while an equilibrium contact time of 30 and 15 min for Cu^{2+} and Pb^{2+}, respectively. As shown in Fig. 5, the removal efficiencies remained high and nearly unchanged for up to 50 mg L^{-1} of both heavy metal ions and decreased by about 50% by increasing the initial concentrations from 50 to 100 mg L^{-1}. The adsorption capacities, however, increased linearly by increasing the initial concentrations of both Cu^{2+} and Pb^{2+} from 5 to 60 mg L^{-1} and remained unchanged afterward up to the maximum used value (100 mg L^{-1}) in this study. Strong driving forces exist between the surface of the LDH/RHB adsorbent and high amount of heavy metal ions [49,50] resulting high adsorption capacities while low removal efficiencies result due to a fixed dose of the LDH/RHB adsorbent (0.4 g) to attract high amount of studied metal ions. Keeping in view the changes in both parameters, 50 mg L^{-1} of both heavy metal ions was considered to be the optimum concentration exhibiting 117 and 124 mg g^{-1} of adsorption capacities for Cu^{2+} and Pb^{2+}, respectively.

Changes in the adsorption capacities and removal efficiencies by varying the solution pH from 2 to79 are depicted in Fig. 5. To optimize the said parameter, 0.4 g of the LDH/RHB adsorbent was used for 50 mg L^{-1} of each heavy metal ion by agitating the tested dilution for 30 and 15 min of equilibrium contact time for Cu^{2+} and Pb^{2+}, respectively. Low percentage removal and adsorption capacities under acidic solution pH (2 – 3) was probably due to the high amount of H^+ presenting more competition to positively charged heavy metal ion to attach to the surface of the LDH/RHB adsorbent. Low H^+ concentrations at high pH values provides more chances for divalent metal ions to attach to the surface of the LDH/RHB adsorbent [51–53] resulting increased adsorption capacities and percentage removal. Precipitation of the tested solutions occur at pH value of 7.0 while a percentage removal of 94% and 99% was recorded at a solution pH value of 6.0 with a maximum adsorption capacity of 117 and 124 mg g^{-1}, respectively, for Cu^{2+} and Pb^{2+}.

Preprints (www.preprints.org) | NOT PEER-REVIEWED | Posted: 22 May 2023 doi:10.20944/preprints202305.1502.v1

3.3. Explanation of the adsorption data using kinetic models

Various commonly used kinetic models were applied to fit the experimental data obtained through batch tests using 30 – 80 mg L^{-1} as initial concentrations of each of the Cu^{2+} and Pb^{2+}. The estimation of parameters in linearized fitting was achieved using the slope and intercept of the fitted line while OriginPro 8.5 Software was used for the same in nonlinear fitting by plotting the adsorption capacity (q_t, mg g^{-1}) against respective retention time (t, min). The original nonlinear expressions of the pseudo first-order (1st-pseudo, Eq. 3), pseudo second-order (2nd-pseudo, Eq. 4), the Elovich (Eq. 5) and the intraparticle diffusion of Weber and Morris (ID-WM, Eq. 6) are as follows;

$$q_t = q_e\,(1 - \exp(-k_1 t)) \tag{3}$$

$$q_t = \frac{{q_e}^2 k_2 . t}{q_e k_2 . t + 1} \tag{4}$$

$$q_t = \frac{1}{\beta}\ln(1 + \alpha\beta t) \tag{5}$$

$$q_t = K_{ip} t^{1/2} + C \tag{6}$$

Table 1 and Table 2 shows the values and comparison of different parameters as calculated in each model for the linearized and nonlinear fitting of each model, respectively. 0.4 g of the LDH/RHB adsorbent was used with a maintained solution pH at 6.0 ± 0.3 while equilibrium adsorption capacities were taken against 30 and 15 min of contact time for Cu^{2+} and Pb^{2+}, respectively, to compare the calculated adsorption capacities (q_e, mg g^{-1}). The rate constants of the 1st-pseudo and 2nd-pseudo kinetic models are expressed by k_1 (min^{-1}) and k_2 (mg g^{-1} min^{-1}) in Eq. 3 and Eq. 4, respectively. In the Elovich kinetic model (Eq. 5), α (mg g^{-1} min^{-1}) and β (g mg^{-1}) represents the respective rate constant and the activation energy, respectively, while K_{ip} (mg g^{-1} $min^{1/2}$) and C (mg g^{-1}) in the ID-WM kinetic model (Eq. 6) represents the respective rate constant and the boundary-layer thickness.

Table 1. Estimation of parameters in linearized kinetic models at various initial concentrations of Cu^{2+} (against 30 min) and Pb^{2+} (against 15 min) onto 0.4 g of the composite adsorbent at pH = 6 ± 0.3.

Kinetic model	Parameter	Initial Cu^{2+} concentrations, mg L^{-1}				Initial Pb^{2+} concentrations, mg L^{-1}			
		30	50	60	80	30	50	60	80
	$q_{e\ exp}$ (mg g^{-1})	72.50	117.12	127.50	127.50	74.98	124.17	135.00	135.00
2nd-pseudo	$q_{e\ cal}$ (mg g^{-1})	71.43	125.00	129.87	128.21	74.63	123.46	135.14	135.14
	k_2 (g mg^{-1} min^{-1})	0.1960	0.0030	0.0037	0.0038	0.138	0.031	0.042	0.012
	h (mg g^{-1} min^{-1})	1000.00	46.95	62.89	62.11	769.23	476.19	769.23	217.39
	R^2	0.9999	0.9996	0.9997	0.9996	1	1	0.9999	0.9999
Elovich	α (mg g^{-1} min^{-1})	1.95E+07	9.79E+01	5.91E+01	2.61E+01	1.45E+18	2.59E+06	2.60E+05	6.44E+04
	β (g mg^{-1})	3.37	13.16	14.66	16.06	1.62	6.48	8.03	8.73
	R^2	0.78	0.9	0.88	0.87	0.53	0.73	0.77	0.75
ID-WM	K_{ip} (mg g^{-1} $min^{1/2}$)	0.98	4.25	4.56	4.97	0.38	1.65	2.08	2.26
	C (mg g^{-1})	59.96	69.71	71.80	65.89	70.42	105.41	111.97	109.52
	R^2	0.49	0.73	0.65	0.63	0.24	0.40	0.43	0.42
1st-pseudo	$q_{e\ cal}$ (mg g^{-1})	3.55	18.62	14.92	13.18	1.05	5.59	5.73	5.83
	k_1 (min^{-1})	0.007	0.015	0.014	0.012	0.008	0.015	0.009	0.010
	R^2	0.22	0.55	0.44	0.28	0.19	0.55	0.29	0.29

In Fig. 6, an illustration of the fitting of both of the linearized and nonlinear types are presented for the selected initial concentrations (50 and 80 mg L^{-1}) of both Cu^{2+} and Pb^{2+} for the 2nd-pseudo and Elovich kinetic models. A perfect fitting of the linearized 2nd-pseudo model can be predicted for all the tested initial concentrations of each heavy metal ion (Fig. 6a and Table 1), based on the estimated values of the coefficient of determination (R^2) as high as 1.0. Nonlinear fitting of the 2nd-pseudo model also yielded high R^2 (0.89 – 0.96, Table 2) for all tested initial concentrations of both heavy metal ions

Preprints (www.preprints.org) | NOT PEER-REVIEWED | Posted: 22 May 2023 doi:10.20944/preprints202305.1502.v1

with the exception of 50 mg L^{-1} of Cu^{2+} (0.77, Fig. 6b). A close match of the experimental and calculated adsorption capacities in the linearized as well as nonlinear 2nd-pseudo model (Table 1 and Table 2, respectively) also suggests that chemisorption can be thought as the controlling mechanism [54–56] for the studied adsorption process. An average R^2 of 0.75 – 0.85 in the linearized as well as nonlinear Elovich kinetic model (except for 30 mg L^{-1} of Pb^{2+} in nonlinear fitting, Table 2) also suggests the fitting of the model to the adsorption data. The model's rate constant (α, mg g^{-1} min^{-1}) decreased as the initial concentrations of either (Cu^{2+} or Pb^{2+}) heavy metal ion increased in both the linearized as well as nonlinear Elovich model. The activation energy (β, g mg^{-1}) increased by increasing the initial concentration of Cu^{2+} or Pb^{2+} in the linearized fitting of the Elovich model (Table 1), whereas an opposite trend (decreasing β. Table 2) can be seen for the nonlinear fitting of the Elovich model as the initial concentration of either Cu^{2+} or Pb^{2+} increased.

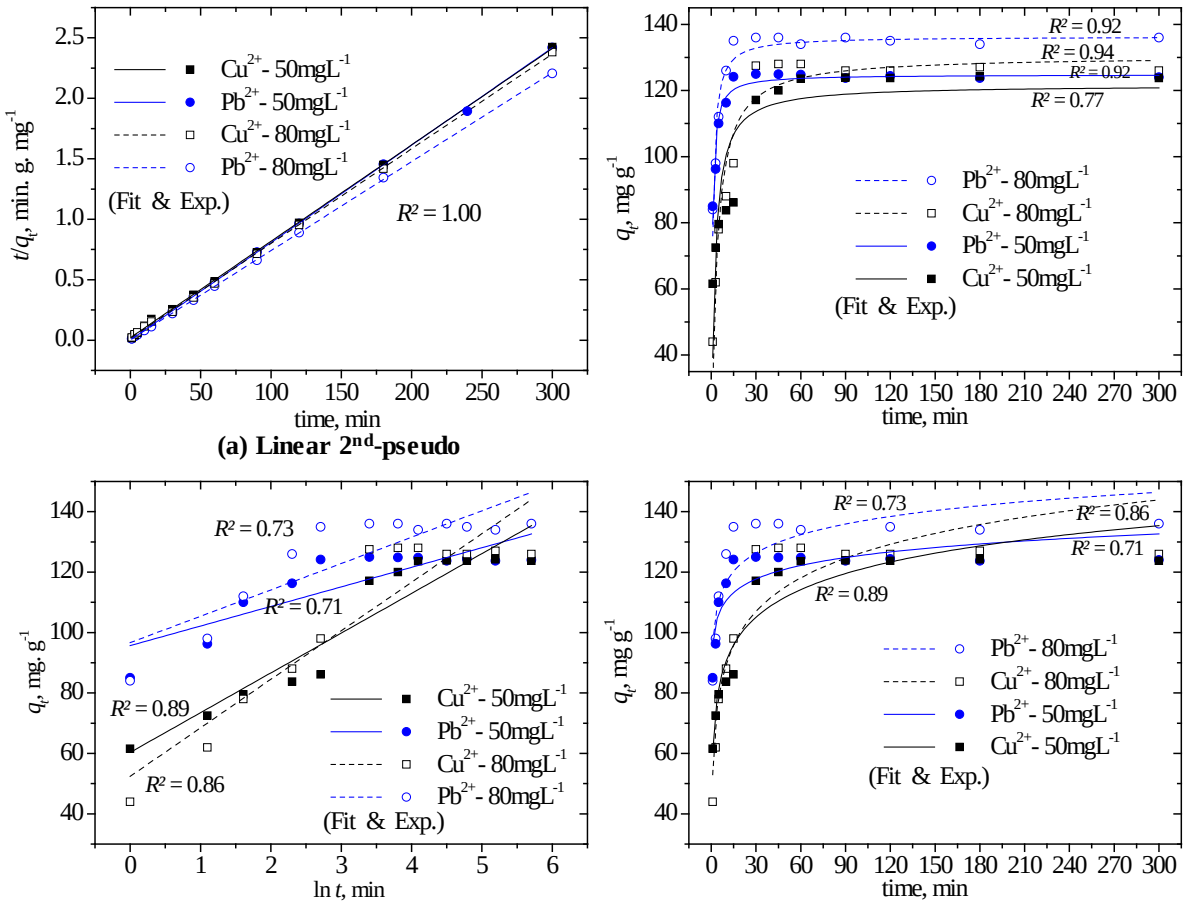

Figure 6. Illustrations of the fitting of the linearized and nonlinear 2nd-pseudo and the Elovich kinetic models at 50 and 80 mg L^{-1} of both heavy metal ions using 0.4 g of the composite compound.

Preprints (www.preprints.org) | NOT PEER-REVIEWED | Posted: 22 May 2023 doi:10.20944/preprints202305.1502.v1

Table 2. Estimation of parameters in nonlinear kinetic models at various initial concentrations of Cu^{2+} (against 30 min) and Pb^{2+} (against 15 min) onto 0.4 g of the composite adsorbent at pH = 6 ± 0.3.

Kinetic model	Parameter	Initial Cu^{2+} concentrations, mg L^{-1}				Initial Pb^{2+} concentrations, mg L^{-1}			
		30	50	60	80	30	50	60	80
	$q_{e\ exp}$ (mg g^{-1})	72.50	117.12	127.50	127.50	74.98	124.17	135.00	135.00
2nd-pseudo	$q_{e\ cal}$ (mg g^{-1})	71.48	121.63	129.78	130.47	75.19	124.81	136.24	136.32
	k_2 (g mg^{-1} min^{-1})	0.030	0.004	0.003	0.002	0.062	0.014	0.011	0.009
	h (mg g^{-1} min^{-1})	153.33	57.99	51.03	40.34	350.10	219.95	202.87	172.26
	R^2	0.90	0.77	0.89	0.94	0.96	0.92	0.89	0.92
Elovich	α (mg g^{-1} min^{-1})	6.60E+07	1.28E+03	8.62E+02	4.20E+02	2.10E+18	1.69E+07	2.08E+06	5.65E+05
	β (g mg^{-1})	0.30	0.08	0.07	0.06	0.62	0.15	0.12	0.11
	R^2	0.76	0.89	0.87	0.86	0.48	0.71	0.74	0.73
ID-WM	K_{ip} (mg g^{-1} $min^{1/2}$)	61.54	75.91	78.66	77.34	70.42	105.41	111.97	109.52
	C (mg g^{-1})	0.87	3.96	4.19	3.05	0.38	1.65	2.08	2.26
	R^2	0.38	0.65	0.56	0.49	0.17	0.34	0.37	0.36
	$q_{e\ cal}$ (mg g^{-1})	69.37	115.34	123.69	124.06	74.17	120.94	131.52	131.86
1st-pseudo	k_1 (min^{-1})	1.23	0.30	0.23	0.18	1.74	1.00	0.88	0.69
	R^2	0.57	0.50	0.73	0.86	0.87	0.64	0.58	0.68

Based on R^2 values, the linearized ID-WM model yielded better fitting results compared with the 1st-pseudo model with the exception of 50 mg L^{-1} of Pb^{2+} (comparative values between two models, Table 1) while the nonlinear fitting yielded opposite results with the exception of 50 mg L^{-1} of Cu^{2+} (Table 2). The rate constant in the ID-WM model and the boundary layer thickness observed an increasing trend with increase in the initial concentrations of respective metal ion with the exception of 80 mg L^{-1} of Cu^{2+}. The rate constant in the nonlinear 1st-pseudo model observed a decreasing trend with increase in the initial concentrations of respective metal ion, as presented in Table 2. Despite the poorest-fit of the linearized 1st-pseudo model (R^2 values in Table 1), the nonlinear fitting yielded a close-match between the experimental and calculated adsorption capacities (Table 2).

3.4. Explanation of the adsorption data using isotherm models

The experimental data of the batch testing is further explained and equilibrium concentrations are analyzed by fitting of commonly used isotherm models which are mentioned in Table 3. These included the Langmuir, Freundlich, Dubinin–Radushkevich (D–R), Temkin, Halsey, and Jovanovic isotherms as two-parameter models and Redlich–Peterson (R–P), and Sips isotherms as three-parameter models. The absorption of both Cu^{2+} and Pb^{2+} to the LDH/RHB adsorbent is explained using the nonlinear as well as linearized (with the exception of three-parameter models) fitting.

Table 3. Mathematical expressions of the two- and three-parameter isotherm models and explanation of parameters.

Isotherm model	Mathematical expression	Parameters
Langmuir	$q_e = \frac{q_m K_L C_e}{(1 + K_L C_e)}$ $R_L = \frac{1}{(1 + K_L C_o)}$	q_m, maximum sorption capacity, mg g^{-1} K_L, Langmuir constant, L mg^{-1} R_L, separation factor coefficient
Freundlich	$q_e = K_F {c_e}^{1/n}$	K_F, Freundlich constant, L g^{-1} n, dimensionless constant
Dubinin–Radushkevich	$q_e = q_m \exp(-K_{DR}\varepsilon^2)$ $\varepsilon = RT \ln(1 + 1/Ce)$ $E = 1/\sqrt{2K_{\ast\ast}}$	T, absolute temperature, Kelvin R, universal gas constant, 8.314 J mol^{-1}·K^{-1} E, mean free energy of adsorption, kJ mol^{-1}
Temkin	$q_e = \frac{RT}{H_{ads}} \ln(K_T\ C_e)$	A_T, equilibrium binding constant, L g^{-1}

Preprints (www.preprints.org) | NOT PEER-REVIEWED | Posted: 22 May 2023 doi:10.20944/preprints202305.1502.v1

		b_T, heat of adsorption, kJ mol^{-1}
Halsey	$q_e = \exp\left(\frac{\ln k_H - \ln C_e}{n_H}\right)$	n_H and k_H, Halsey constants
Jovanovic	$q_e = q_m\,[1 - \exp(k_j C_e)]$	k_j, Jovanovic constant
Redlich–Peterson	$q_e = \frac{K_{RP} C_e}{1 + \alpha {C_e}^{\beta}}$	α, L mg^{-1} β (0–1), dimensionless K_{RP}, R–P constant, L g^{-1}
Sips	$q_e = \frac{q_m K_S {C_e}^{n_s}}{1 + K_S {C_e}^{n_s}}$	n_s, degree of heterogeneity, dimensionless K_S, energy of adsorption, L g^{-1}

Theoretical adsorption capacities were computed in different models and compared with the experimental values at 30 and 15 min of equilibrium time for 60 mg L^{-1} of each Cu^{2+} and Pb^{2+}, respectively. The initial concentration of the selected metal ions ranged between 5 and 100 mg L^{-1} for the batch testing using 0.4 g of the LDH/RHB adsorbent by maintaining the dilution pH at 6.0±0.3. Estimation of parameters (presented in Table 4) in each model is based on the slope and intercept of the linearized fitting to the experimental data while for the nonlinear fitting, OriginPro 8.5 Software was used to calculate the parameters of each model based on the fit to the plot of the experimental adsorption capacity (q_e, mg g^{-1}) and respective residual concentration (C_e, mg L^{-1}). Fig. 7 illustrates the linearized as well as nonlinear fitting of selected models based on most favorable and commonly employed isotherms.

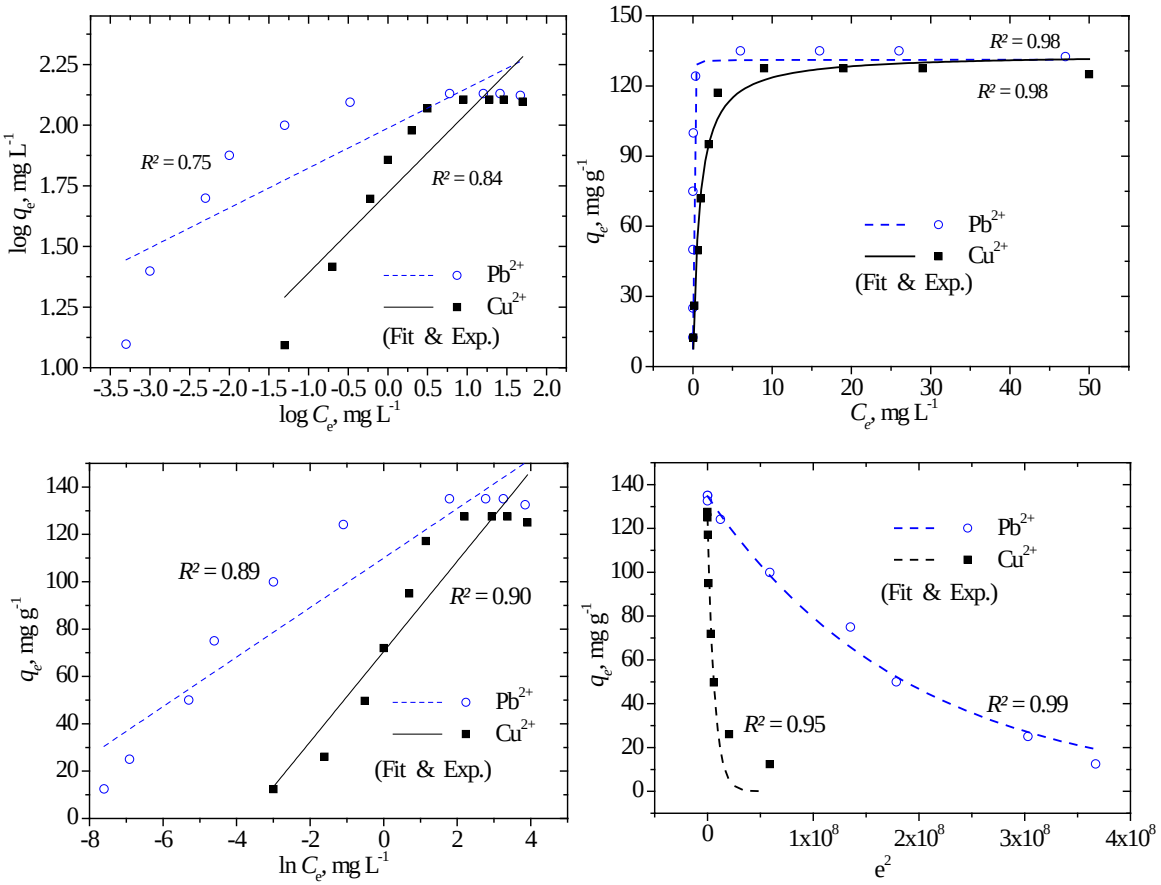

Figure 7. Illustrations of the linearized and nonlinear fitting of the selected isotherm models to the adsorption data of both heavy metal ions using the composite compound.

Linearized as well as nonlinear fitting (Fig. 7b) of the Langmuir model yielded a near to perfect-fit to the adsorption of both heavy metal ions on to the LDH/RHB adsorbent with significant high R^2 (0.97 – 0.99), as presented in Table 4, supporting a monolayer sorption of both heavy metal ions to a

Preprints (www.preprints.org) | NOT PEER-REVIEWED | Posted: 22 May 2023 doi:10.20944/preprints202305.1502.v1

fixed number of homogeneous sorption sites on the surface of the LDH/RHB adsorbent. A favorable adsorption is indicated based on the calculated values of the separation factor coefficient (R_L less than 1.0, Table 4) [57] with a quite higher Langmuir constant value for Pb^{2+} compared with Cu^{2+}. The calculated adsorption capacities were lower than the experimental values in linearized approach but matched closely in case of nonlinear Langmuir isotherm, as presented in Table 4. The Freundlich model did not yield better fit to the adsorption data compared with the Temkin or D–R isotherms (comparison of R^2 values in Table 4) in addition to significantly high estimation of theoretical adsorption capacities comparing to the experimental values especially when using the linearized approach. Higher Freundlich constant and degree of site heterogeneity ($1/n$ closer to zero) was estimated for Pb^{2+} compared to Cu^{2+} (K_F in Table 4) whereas the adsorption process is estimated to be chemisorption based on $1/n$ values (less than 1.0, Table 4).

Table 4. Estimation of parameters in linearized and nonlinear isotherm models against 60 mg L^{-1} of both heavy metal ions (solution pH= 6±0.3, contact time = 30 and 15 min for Cu^{2+} and Pb^{2+}, respectively, and adsorbent dose = 0.4 g).

Isotherm	Parameter	*Linearized fitting*		*Nonlinear fit*	
		Cu^{2+}	**Pb^{2+}**	**Cu^{2+}**	**Pb^{2+}**
	$q_{e\ exp}$, mg g^{-1}	**127.53**	**135**	**127.53**	**135**
Langmuir	q_m, mg g^{-1}	102.04	119.05	133.64	131.21
	K_L, L mg^{-1}	2.65	210.00	1.23	125.29
	R_L	0.006	0.00008	0.013	0.00013
	R^2	0.97	0.99	0.98	0.98
Freundlich	q_m, mg g^{-1}	238.54	197.17	153.72	154.81
	K_F, ((mg/g)(L/mg)$^{1/n}$)	61.74	100.54	68.51	101.70
	$1/n$	0.330	0.165	0.197	0.103
	R^2	0.84	0.75	0.77	0.77
D–R	q_m, mg g^{-1}	102.51	139.49	124.64	134.71
	K_{DR}, (mol $kJ^{-1})^2$	4.0E-08	6.0E-09	1.54E-07	5.3E-09
	E, kJ mol^{-1}	3.54	7.13	1.80	7.71
	R^2	0.85	0.98	0.95	0.99
Temkin	K_T, L mg^{-1}	40.46	370.33	40.46	370.53
	H_{ads}, kJ mol^{-1}	132.23	241.05	132.22	241.04
	R^2	0.90	0.89	0.89	0.88
Halsey	$q_{e\ cal}$, mg g^{-1}	258.10	217.21	122.50	135.17
	n_H	-3.03	-6.08	-5.07	-9.75
	K_H	0.465	0.265	0.023	0.012
	R^2	0.84	0.75	0.77	0.77
Jovanovic	q_m, mg g^{-1}	53.34	58.04	126.29	127.28
	k_j, L g^{-1}	-0.025	-0.025	-0.82	-4.15
	R^2	0.27	0.23	0.99	0.94
R–P	K_{RP}, L g^{-1}			125.13	213.36
	α, L mg^{-1}			0.73	1.47
	β			1.08	0.98
	R^2			0.99	0.99
Sips	q_m, mg g^{-1}			130.86	134.82
	K_S, L g^{-1}			1.30	2.39
	n_S			1.17	0.70
	R^2			0.98	1.00

The adsorption of Cu^{2+} and Pb^{2+} to the LDH/RHB adsorbent seems to be a physical adsorption, as suggested by the calculated E values in D–R isotherm (<8 kJ mol^{-1}, Table 4) using the linearized as well as nonlinear approach. A perfect fit of the model is also evident from the high R^2 values (0.95 – 0.99, Fig. 7d) for the nonlinear fitting and through a close match of the calculated and experimental adsorption capacities with the exception of Cu^{2+} using only linearized fitting (103 mg g^{-1} against 127 mg g^{-1}, Table 4). D–R isotherm exhibited lower K_{DR} and in turn higher mean free energy of adsorption for Pb^{2+} compared with Cu^{2+} (E values in Table 4). The Temkin isotherm also predicted a reasonable fit of the adsorption data with an average R^2 value of 0.9 (Fig. 7c and Table 4) suggesting a heterogeneous adsorption of both heavy metal ions with uniform dispersal of binding energies on the surface of the

Preprints (www.preprints.org) | NOT PEER-REVIEWED | Posted: 22 May 2023 doi:10.20944/preprints202305.1502.v1

LDH/RHB adsorbent [58]. Pb^{2+} exhibited higher heat of adsorption compared with Cu^{2+} while both linearized and nonlinear fitting yielded same results for the respective values of equilibrium binding constant and heat of adsorption. Both Halsey and Jovanovic isotherms yielded a close match of the calculated adsorption capacities to the experimental values using the nonlinear fitting with lower values of the model's constants for Pb^{2+} in comparison to Cu^{2+}. A poor-fit of the linearized Jovanovic model was seen based on R^2 values (0.23 – 0.27, Table 4) while a very good fit of the nonlinear Jovanovic model was observed with high R^2 values (0.94 – 0.99, Table 4) better than the Halsey isotherm with an average R^2 value of 0.77, as presented in Table 4. The homogeneous as well as heterogeneous adsorption of both Cu^{2+} and Pb^{2+} to the LDH/RHB adsorbent is also proposed by three-parameter model [59–62] since a near to prefect-fit of the Sips and R–P isotherms was predicted based on very high R^2 values (0.98 – 1.00, Table 4) for both heavy metal ions using the nonlinear approach. The findings of the Sips model suggested a lower degree of heterogeneity and higher heat of adsorption for Pb^{2+} compared with Cu^{2+} (comparison of n_s and K_S values in Table 4) with a close match of the calculated and experimental adsorption capacities.

4. Conclusions

A new composite material of ZnMgAl(LDH) and RHB using the co-precipitation and hydrothermal technique was developed in this study and the removal mechanisms of Cu(II) and Pb(II) ions from synthetic wastewater was investigated. Extensive batch tests were conducted and the kinetics and isothermal models were deployed to understand the removal mechanisms and to calculate the adsorption capacity of the composite material. SEM micrographs of the LDH/RHB composite showed extremely fine crystalline LDH particles decorated on the rough surface of the RHB while the succesful formation of the composite adsorbent was confirmed by the corresponding EDX spectrum of the composite displayings all bonding elements that were present separately in the RHB and ZnMgAl(LDH) spectra. Further, the EDX spectra of the composite adsorbent after the adsorption of studied heavy metal ions, showed many variations in elemental composition in addition to the presence of Cu (3.41%) and Pb (47.63%) indicating successful absorption of the target metals into LDH/RHB composites. The effective synthesis of the composite adsorbent was further evident from the FTIR spectrum which also suggested a change (low intensity) or vanishing nitrate and hydroxyl representing bands with a possible replacement by $Cu^{2+}$and Pb^{2+}.

A rapid uptake of each heavy metal ion upon immediate contact with the adsorbent was observed following a steady increase afterwards until 30 and 15 min for Cu^{2+} and Pb^{2+}, respectively, proposing, thus a different equilibrium contact time for Cu^{2+} and Pb^{2+}. Furthermore, the composite adsorbent exhibited slightly higher adsorption capacity and removal efficiency for Pb^{2+} in comparison to Cu^{2+}. A steady increase in the adsorption capacity by increasing the amount of the adsorbent was observed with maximum values of 117 and 124 mg g^{-1} for Cu^{2+} and Pb^{2+}, respectively, at 0.4 g of the tested dose. The corresponding maximum removal efficiency was about 94% and 99% for Cu^{2+} and Pb^{2+}, respectively, at 0.4 g of the LDH/RHB adsorbent. For the changing initial metal's concentration, the removal efficiencies remained unchanged for up to 50 mg L^{-1} and decreased by about 50% by increasing the initial concentrations from 50 to 100 mg L^{-1}. The adsorption capacities observed a linear increasing trend by increasing the initial concentrations from 5 to 60 mg L^{-1} and remained unchanged afterward up to 100 mg L^{-1}. An increase in the adsorption capacities and percentage removal was observed by changing the solution pH from 2.0 to 6.0 a observing a maximum adsorption capacity of 117 and 124 mg g^{-1} for Cu^{2+} and Pb^{2+}, respectively.

With a perfect fitting of the linearized 2nd-pseudo model (R^2 as high as 1.0) as well as of the nonlinear fitting (R^2 as high as 0.89 – 0.96) for all tested initial concentrations of both heavy metal ions and of a close match of the experimental and calculated adsorption capacities, the chemisorption was suggested to be the controlling mechanism. Among the isotherm models, the a near to perfect-fit (R^2 as high as 0.97 – 0.99) of the linearized as well as nonlinear Langmuir model to the experimental data, a monolayer sorption of both heavy metal ions to a fixed number of homogeneous sorption sites on the surface of the LDH/RHB adsorbent can be proposed. A heterogeneous adsorption of both heavy metal ions with uniform dispersal of binding energies on the surface of the LDH/RHB adsorbent can

Preprints (www.preprints.org) | NOT PEER-REVIEWED | Posted: 22 May 2023 doi:10.20944/preprints202305.1502.v1

also be proposed based on a reasonable fit (with an average R^2 value of 0.9) of the Temkin isotherm to the experimental data. The application of the D–R isotherm with high R^2 values (0.95 – 0.99) helped to conclude the adsorption of Cu^{2+} and Pb^{2+} to the LDH/RHB adsorbent a physical adsorption with estimated E values less than 8 kJ mol^{-1}. The idea of both homogeneous as well as heterogeneous adsorption of both heavy metal ions to the LDH/RHB adsorbent is further supported by a perfect-fit (R^2 values in the range 0.98 – 1.00) of the Sips and R–P isotherms (three-parameter models) to the experimental data. A close match of the calculated and experimental adsorption capacities was seen using the Sips isotherm with a lower degree of heterogeneity and higher heat of adsorption for Pb^{2+} compared with Cu^{2+}.

Acknowledgments: The project was financially supported by the Vice Deanship of Research Chairs, King Saud University, Riyadh, KSA.

Conflicts of Interest: The authors declare no conflict of interest.

References

1. Zhou, Q.; Liao, B.; Lin, L.; Qiu, W.; Song, Z. Adsorption of Cu(II) and Cd(II) from Aqueous Solutions by Ferromanganese Binary Oxide–Biochar Composites. *Science of The Total Environment* **2018**, *615*, 115–122, doi:10.1016/j.scitotenv.2017.09.220.
2. Ye, L.; Chai, L.; Li, Q.; Yan, X.; Wang, Q.; Liu, H. Chemical Precipitation Granular Sludge (CPGS) Formation for Copper Removal from Wastewater. *RSC Adv.* **2016**, *6*, 114405–114411, doi:10.1039/C6RA11165C.
3. Zhou, H.; Tan, Y.; Gao, W.; Zhang, Y.; Yang, Y. Removal of Copper Ions from Aqueous Solution by a Hydrotalcite-Like Absorbent FeMnMg-LDH. *Water Air Soil Pollut* **2020**, *231*, 370, doi:10.1007/s11270-020-04714-8.
4. Wang, T.; Li, C.; Wang, C.; Wang, H. Biochar/MnAl-LDH Composites for Cu (II) Removal from Aqueous Solution. *Colloids and Surfaces A: Physicochemical and Engineering Aspects* **2018**, *538*, 443–450, doi:10.1016/j.colsurfa.2017.11.034.
5. Jayashree, S.; Ramesh, S.T.; Lavanya, A.; Gandhimathi, R.; Nidheesh, P.V. Wastewater Treatment by Microbial Fuel Cell Coupled with Peroxicoagulation Process. *Clean Techn Environ Policy* **2019**, *21*, 2033–2045, doi:10.1007/s10098-019-01759-0.
6. Salazar, R.; Gallardo-Arriaza, J.; Vidal, J.; Rivera-Vera, C.; Toledo-Neira, C.; Sandoval, M.A.; Cornejo-Ponce, L.; Thiam, A. Treatment of Industrial Textile Wastewater by the Solar Photoelectro-Fenton Process: Influence of Solar Radiation and Applied Current. *Solar Energy* **2019**, *190*, 82–91, doi:10.1016/j.solener.2019.07.072.
7. Obotey Ezugbe, E.; Rathilal, S. Membrane Technologies in Wastewater Treatment: A Review. *Membranes (Basel)* **2020**, *10*, 89, doi:10.3390/membranes10050089.
8. Pohl, A. Removal of Heavy Metal Ions from Water and Wastewaters by Sulfur-Containing Precipitation Agents. *Water Air Soil Pollut* **2020**, *231*, 503, doi:10.1007/s11270-020-04863-w.
9. Barakat, M.A. New Trends in Removing Heavy Metals from Industrial Wastewater. *Arabian Journal of Chemistry* **2011**, *4*, 361–377, doi:10.1016/j.arabjc.2010.07.019.
10. Amin, M.T.; Alazba, A.A.; Shafiq, M. Comparative Removal of Lead and Nickel Ions onto Nanofibrous Sheet of Activated Polyacrylonitrile in Batch Adsorption and Application of Conventional Kinetic and Isotherm Models. *Membranes* **2021**, *11*, 10, doi:10.3390/membranes11010010.
11. Batool, S.; Idrees, M.; Hussain, Q.; Kong, J. Adsorption of Copper (II) by Using Derived-Farmyard and Poultry Manure Biochars: Efficiency and Mechanism. *Chemical Physics Letters* **2017**, *689*, 190–198, doi:10.1016/j.cplett.2017.10.016.
12. Rojas, R. Copper, Lead and Cadmium Removal by Ca Al Layered Double Hydroxides. *Applied Clay Science* **2014**, *87*, 254–259, doi:10.1016/j.clay.2013.11.015.
13. Amin, M.T.; Alazba, A.A.; Shafiq, M. Removal of Copper and Lead Using Banana Biochar in Batch Adsorption Systems: Isotherms and Kinetic Studies. *Arab J Sci Eng* **2017**, 1–12, doi:10.1007/s13369-017-2934-z.
14. Ahmad, M.; Ahmad, M.; Usman, A.R.A.; Al-Faraj, A.S.; Abduljabbar, A.S.; Al-Wabel, M.I. Biochar Composites with Nano Zerovalent Iron and Eggshell Powder for Nitrate Removal from Aqueous Solution with Coexisting Chloride Ions. *Environ Sci Pollut Res Int* **2017**, doi:10.1007/s11356-017-0125-9.
15. Kinoti, I.K.; Karanja, E.M.; Nthiga, E.W.; M'thiruaine, C.M.; Marangu, J.M. Review of Clay-Based Nanocomposites as Adsorbents for the Removal of Heavy Metals. *Journal of Chemistry* **2022**, *2022*, e7504626, doi:10.1155/2022/7504626.

Preprints (www.preprints.org) | NOT PEER-REVIEWED | Posted: 22 May 2023 doi:10.20944/preprints202305.1502.v1

16. Shafiq, M.; Alazba, A.A.; Amin, M.T. Adsorption of Divalent Copper Ions from Synthetic Wastewater Using Layered Double Hydroxides (NiZnFe) and Its Composites with Banana Biochar and Carbon Nanotubes. *Water Air Soil Pollut* **2020**, *231*, 346, doi:10.1007/s11270-020-04732-6.
17. Ethaib, S.; Al-Qutaifia, S.; Al-Ansari, N.; Zubaidi, S.L. Function of Nanomaterials in Removing Heavy Metals for Water and Wastewater Remediation: A Review. *Environments* **2022**, *9*, 123, doi:10.3390/environments9100123.
18. Yang, J.; Hou, B.; Wang, J.; Tian, B.; Bi, J.; Wang, N.; Li, X.; Huang, X. Nanomaterials for the Removal of Heavy Metals from Wastewater. *Nanomaterials* **2019**, *9*, doi:10.3390/nano9030424.
19. Stoian, O.; Covaliu, C.I.; Paraschiv, G.; Catrina (Traistaru), G.-A.; Niță-Lazăr, M.; Matei, E.; Biriş, S. Ștefan; Tudor, P. Magnetite Oxide Nanomaterial Used for Lead Ions Removal from Industrial Wastewater. *Materials (Basel)* **2021**, *14*, 2831, doi:10.3390/ma14112831.
20. Do Minh, T.; Song, J.; Deb, A.; Cha, L.; Srivastava, V.; Sillanpää, M. Biochar Based Catalysts for the Abatement of Emerging Pollutants: A Review. *Chemical Engineering Journal* **2020**, *394*, 124856, doi:10.1016/j.cej.2020.124856.
21. Bhatnagar, A.; Sillanpää, M. Utilization of Agro-Industrial and Municipal Waste Materials as Potential Adsorbents for Water Treatment—A Review. *Chemical Engineering Journal* **2010**, *157*, 277–296, doi:10.1016/j.cej.2010.01.007.
22. Kumar, P.S.; Gayathri, R.; Rathi, B.S. A Review on Adsorptive Separation of Toxic Metals from Aquatic System Using Biochar Produced from Agro-Waste. *Chemosphere* **2021**, *285*, 131438, doi:10.1016/j.chemosphere.2021.131438.
23. Wijeyawardana, P.; Nanayakkara, N.; Gunasekara, C.; Karunarathna, A.; Law, D.; Pramanik, B.K. Removal of Cu, Pb and Zn from Stormwater Using an Industrially Manufactured Sawdust and Paddy Husk Derived Biochar. *Environmental Technology & Innovation* **2022**, *28*, 102640, doi:10.1016/j.eti.2022.102640.
24. Sanka, P.M.; Rwiza, M.J.; Mtei, K.M. Removal of Selected Heavy Metal Ions from Industrial Wastewater Using Rice and Corn Husk Biochar. *Water Air Soil Pollut* **2020**, *231*, 244, doi:10.1007/s11270-020-04624-9.
25. Han, W.; Hao, H.; Zhang, Q.; Shao, Z. Activated Biochar Loaded CuAl-Layered Double Hydroxide Composite for the Removal of Aniline Aerofloat in Wastewater: Synthesis, Characterization, and Adsorption Mechanism. *Journal of Environmental Chemical Engineering* **2023**, 109293, doi:10.1016/j.jece.2023.109293.
26. Fang, Q.; Ye, S.; Yang, H.; Yang, K.; Zhou, J.; Gao, Y.; Lin, Q.; Tan, X.; Yang, Z. Application of Layered Double Hydroxide-Biochar Composites in Wastewater Treatment: Recent Trends, Modification Strategies, and Outlook. *Journal of Hazardous Materials* **2021**, *420*, 126569, doi:10.1016/j.jhazmat.2021.126569.
27. Zhu, L.; Meng, L.; Shi, J.; Li, J.; Zhang, X.; Feng, M. Metal-Organic Frameworks/Carbon-Based Materials for Environmental Remediation: A State-of-the-Art Mini-Review. *Journal of Environmental Management* **2019**, *232*, 964–977, doi:10.1016/j.jenvman.2018.12.004.
28. Musarurwa, H.; Tavengwa, N.T. Smart Metal-Organic Framework (MOF) Composites and Their Applications in Environmental Remediation. *Materials Today Communications* **2022**, *33*, 104823, doi:10.1016/j.mtcomm.2022.104823.
29. Johnston, A.-L.; Lester, E.; Williams, O.; Gomes, R.L. Understanding Layered Double Hydroxide Properties as Sorbent Materials for Removing Organic Pollutants from Environmental Waters. *Journal of Environmental Chemical Engineering* **2021**, *9*, 105197, doi:10.1016/j.jece.2021.105197.
30. Wang, R.; Yu, Y.; Zhang, R.; Ren, X.; Guo, W. Engineering the Morphology on Layered Double Hydroxides-Induced Persulfate Activation for Enhanced Degradation of Organic Pollutant 2022.
31. Chubar, N.; Gilmour, R.; Gerda, V.; Mičušík, M.; Omastova, M.; Heister, K.; Man, P.; Fraissard, J.; Zaitsev, V. Layered Double Hydroxides as the next Generation Inorganic Anion Exchangers: Synthetic Methods versus Applicability. *Advances in Colloid and Interface Science* **2017**, *245*, 62–80, doi:10.1016/j.cis.2017.04.013.
32. Fang, Q.; Ye, S.; Yang, H.; Yang, K.; Zhou, J.; Gao, Y.; Lin, Q.; Tan, X.; Yang, Z. Application of Layered Double Hydroxide-Biochar Composites in Wastewater Treatment: Recent Trends, Modification Strategies, and Outlook. *Journal of Hazardous Materials* **2021**, *420*, 126569, doi:10.1016/j.jhazmat.2021.126569.
33. Shao, P.; Yin, H.; Li, Y.; Cai, Y.; Yan, C.; Yuan, Y.; Dang, Z. Remediation of Cu and As Contaminated Water and Soil Utilizing Biochar Supported Layered Double Hydroxide: Mechanisms and Soil Environment Altering. *Journal of Environmental Sciences* **2023**, *126*, 275–286, doi:10.1016/j.jes.2022.05.025.
34. Tan, Y.; Wan, X.; Zhou, T.; Wang, L.; Yin, X.; Ma, A.; Wang, N. Novel Zn-Fe Engineered Kiwi Branch Biochar for the Removal of Pb(II) from Aqueous Solution. *Journal of Hazardous Materials* **2022**, *424*, 127349, doi:10.1016/j.jhazmat.2021.127349.
35. Jia, Y.; Zhang, Y.; Fu, J.; Yuan, L.; Li, Z.; Liu, C.; Zhao, D.; Wang, X. A Novel Magnetic Biochar/MgFe-Layered Double Hydroxides Composite Removing Pb2+ from Aqueous Solution: Isotherms, Kinetics and Thermodynamics. *Colloids and Surfaces A: Physicochemical and Engineering Aspects* **2019**, *567*, 278–287, doi:10.1016/j.colsurfa.2019.01.064.

Preprints (www.preprints.org) | NOT PEER-REVIEWED | Posted: 22 May 2023 doi:10.20944/preprints202305.1502.v1

36. Khandaker, S.; Hossain, M.T.; Saha, P.K.; Rayhan, U.; Islam, A.; Choudhury, T.R.; Awual, Md.R. Functionalized Layered Double Hydroxides Composite Bio-Adsorbent for Efficient Copper(II) Ion Encapsulation from Wastewater. *Journal of Environmental Management* **2021**, *300*, 113782, doi:10.1016/j.jenvman.2021.113782.
37. Saravanan, P.; Josephraj, J.; Thillainayagam, B.P.; Ravindiran, G. Evaluation of the Adsorptive Removal of Cationic Dyes by Greening Biochar Derived from Agricultural Bio-Waste of Rice Husk. *Biomass Conv. Bioref.* **2021**, doi:10.1007/s13399-021-01415-y.
38. Wang, X.; Zhu, X.; Meng, X. Preparation of a Mg/Al/Fe Layered Supramolecular Compound and Application for Removal of Cr(VI) from Laboratory Wastewater. *RSC Adv.* **2017**, *7*, 34984–34993, doi:10.1039/C7RA04646D.
39. Rashed, S.H.; Abd-Elhamid, A.I.; Abdalkarim, S.Y.H.; El-Sayed, R.H.; El-Bardan, A.A.; Soliman, H.M.A.; Nayl, A.A. Preparation and Characterization of Layered-Double Hydroxides Decorated on Graphene Oxide for Dye Removal from Aqueous Solution. *Journal of Materials Research and Technology* **2022**, *17*, 2782–2795, doi:10.1016/j.jmrt.2022.02.040.
40. Park, M.; Choi, C.L.; Seo, Y.J.; Yeo, S.K.; Choi, J.; Komarneni, S.; Lee, J.H. Reactions of Cu2+ and Pb2+ with Mg/Al Layered Double Hydroxide. *Applied Clay Science* **2007**, *37*, 143–148, doi:10.1016/j.clay.2006.12.006.
41. Tan, Y.; Yin, X.; Wang, C.; Sun, H.; Ma, A.; Zhang, G.; Wang, N. Sorption of Cadmium onto Mg-Fe Layered Double Hydroxide (LDH)-Kiwi Branch Biochar. *Environmental Pollutants and Bioavailability* **2019**, *31*, 189–197, doi:10.1080/26395940.2019.1604165.
42. Liang, X.; Zang, Y.; Xu, Y.; Tan, X.; Hou, W.; Wang, L.; Sun, Y. Sorption of Metal Cations on Layered Double Hydroxides. *Colloids and Surfaces A: Physicochemical and Engineering Aspects* **2013**, *433*, 122–131, doi:10.1016/j.colsurfa.2013.05.006.
43. Ma, X.; Li, S.; Ren, H.; Zhang, Y.; Ma, Z. Egg White-Mediated Fabrication of Mg/Al-LDH-Hard Biochar Composite for Phosphate Adsorption. *Molecules* **2022**, *27*, 8951, doi:10.3390/molecules27248951.
44. Li, Z.; Su, Q.; Xiang, L.; Yuan, Y.; Tu, S. Effect of Pyrolysis Temperature on the Sorption of Cd(II) and Se(IV) by Rice Husk Biochar. *Plants* **2022**, *11*, 3234, doi:10.3390/plants11233234.
45. Khitous, M.; Salem, Z.; Halliche, D. Removal of Phosphate from Industrial Wastewater Using Uncalcined MgAl-NO3 Layered Double Hydroxide: Batch Study and Modeling. *Desalination and Water Treatment* **2016**, *57*, 15920–15931, doi:10.1080/19443994.2015.1077745.
46. Palapa, N.R.; Juleanti, N.; Normah; Mohadi, R.; Taher, T.; Rachmat, A.; Lesbani, A. Copper Aluminum Layered Double Hydroxide Modified by Biochar and Its Application as an Adsorbent for Procion Red. *J. of Wat. & Envir. Tech.* **2020**, *18*, 359–371, doi:10.2965/jwet.20-059.
47. Hoang, L.P.; Nguyen, T.M.P.; Van, H.T.; Yılmaz, M.; Hoang, T.K.; Nguyen, Q.T.; Vi, T.M.H.; Nga, L.T.Q. Removal of Tetracycline from Aqueous Solution Using Composite Adsorbent of ZnAl Layered Double Hydroxide and Bagasse Biochar. *Environmental Technology & Innovation* **2022**, *28*, 102914, doi:10.1016/j.eti.2022.102914.
48. Dalla Nora, F.B.; Lima, V.V.C.; Oliveira, M.L.S.; Hosseini-Bandegharaei, A.; de Lima Burgo, T.A.; Meili, L.; Dotto, G.L. Adsorptive Potential of Zn–Al and Mg–Fe Layered Double Hydroxides for the Removal of 2–Nitrophenol from Aqueous Solutions. *Journal of Environmental Chemical Engineering* **2020**, *8*, 103913, doi:10.1016/j.jece.2020.103913.
49. Karapinar, N.; Donat, R. Adsorption Behaviour of Cu2+ and Cd2+ onto Natural Bentonite. *Desalination* **2009**, *249*, 123–129, doi:10.1016/j.desal.2008.12.046.
50. Raji, F.; Pakizeh, M. Study of Hg(II) Species Removal from Aqueous Solution Using Hybrid ZnCl2-MCM-41 Adsorbent. *Applied Surface Science* **2013**, *282*, 415–424, doi:10.1016/j.apsusc.2013.05.145.
51. Tang, H.; Zhou, W.; Zhang, L. Adsorption Isotherms and Kinetics Studies of Malachite Green on Chitin Hydrogels. *J. Hazard. Mater.* **2012**, *209–210*, 218–225, doi:10.1016/j.jhazmat.2012.01.010.
52. Chowdhury, S.; Mishra, R.; Saha, P.; Kushwaha, P. Adsorption Thermodynamics, Kinetics and Isosteric Heat of Adsorption of Malachite Green onto Chemically Modified Rice Husk. *Desalination* **2011**, *265*, 159–168, doi:10.1016/j.desal.2010.07.047.
53. Taty-Costodes, V.C.; Fauduet, H.; Porte, C.; Delacroix, A. Removal of Cd(II) and Pb(II) Ions, from Aqueous Solutions, by Adsorption onto Sawdust of Pinus Sylvestris. *Journal of Hazardous Materials* **2003**, *105*, 121–142, doi:10.1016/j.jhazmat.2003.07.009.
54. Hameed, B.H.; El-Khaiary, M.I. Batch Removal of Malachite Green from Aqueous Solutions by Adsorption on Oil Palm Trunk Fibre: Equilibrium Isotherms and Kinetic Studies. *Journal of Hazardous Materials* **2008**, *154*, 237–244, doi:10.1016/j.jhazmat.2007.10.017.
55. Ayranci, E.; Duman, O. Structural Effects on the Interactions of Benzene and Naphthalene Sulfonates with Activated Carbon Cloth during Adsorption from Aqueous Solutions. *Chemical Engineering Journal* **2010**, *156*, 70–76, doi:10.1016/j.cej.2009.09.038.

Preprints (www.preprints.org) | NOT PEER-REVIEWED | Posted: 22 May 2023 doi:10.20944/preprints202305.1502.v1

56. Duman, O.; Özcan, C.; Gürkan Polat, T.; Tunç, S. Carbon Nanotube-Based Magnetic and Non-Magnetic Adsorbents for the High-Efficiency Removal of Diquat Dibromide Herbicide from Water: OMWCNT, OMWCNT-Fe3O4 and OMWCNT-κ-Carrageenan-Fe3O4 Nanocomposites. *Environmental Pollution* **2019**, *244*, 723–732, doi:10.1016/j.envpol.2018.10.071.
57. Foo, K.Y.; Hameed, B.H. Insights into the Modeling of Adsorption Isotherm Systems. *Chemical Engineering Journal* **2010**, *156*, 2–10, doi:10.1016/j.cej.2009.09.013.
58. Kumar, P.S.; Ramakrishnan, K.; Gayathri, R. Removal of Nickel(II) from Aqueous Solutions by Ceralite IR 120 Cationic Exchange Resins. *Journal of Engineering Science and Technology* **2010**, *5*, 232–243.
59. Gimbert, F.; Morin-Crini, N.; Renault, F.; Badot, P.-M.; Crini, G. Adsorption Isotherm Models for Dye Removal by Cationized Starch-Based Material in a Single Component System: Error Analysis. *Journal of Hazardous Materials* **2008**, *157*, 34–46, doi:10.1016/j.jhazmat.2007.12.072.
60. Abtahi, M.; Mesdaghinia, A.; Saeedi, R.; Nazmara, S. Biosorption of As(III) and As(V) from Aqueous Solutions by Brown Macroalga Colpomenia Sinuosa Biomass: Kinetic and Equilibrium Studies. *Desalination and Water Treatment* **2013**, *51*, 3224–3232, doi:10.1080/19443994.2012.749034.
61. Naddafi, K.; Rastkari, N.; Nabizadeh, R.; Saeedi, R.; Gholami, M.; Sarkhosh, M. Adsorption of 2,4,6-Trichlorophenol from Aqueous Solutions by a Surfactant-Modified Zeolitic Tuff: Batch and Continuous Studies. *Desalination and Water Treatment* **2016**, *57*, 5789–5799, doi:10.1080/19443994.2015.1005693.
62. Günay, A.; Arslankaya, E.; Tosun, İ. Lead Removal from Aqueous Solution by Natural and Pretreated Clinoptilolite: Adsorption Equilibrium and Kinetics. *Journal of Hazardous Materials* **2007**, *146*, 362–371, doi:10.1016/j.jhazmat.2006.12.034.

Disclaimer/Publisher's Note: The statements, opinions and data contained in all publications are solely those of the individual author(s) and contributor(s) and not of MDPI and/or the editor(s). MDPI and/or the editor(s) disclaim responsibility for any injury to people or property resulting from any ideas, methods, instructions or products referred to in the content.